

Article

Decolorization and Oxidation of Acid Blue 80 in Homogeneous and Heterogeneous Phases by Selected AOP Processes

Jiří Palarčík¹, Olga Krupková¹, Petra Peroutková¹, Jan Malaťák² , Jan Velebil², Jaromíra Chýlková¹ and Libor Dušek^{1,*} 

- ¹ Institute of Environmental and Chemical Engineering, Faculty of Chemical Technology, University of Pardubice, Studentská 573, 532 10 Pardubice, Czech Republic; jiri.palarcik@upce.cz (J.P.); olga.krupkova@student.upce.cz (O.K.); petra.peroutkova@upce.cz (P.P.); jaromira.chylkova@upce.cz (J.C.)
- ² Department of Technological Equipment of Buildings, Faculty of Engineering, Czech University of Life Sciences Prague, Kamýcká 129, 165 21 Prague, Czech Republic; malatak@tf.czu.cz (J.M.); velebil@tf.czu.cz (J.V.)
- * Correspondence: libor.dusek@upce.cz; Tel.: +420-466-038-051

Abstract: This paper is a kinetic study that compares the rate of decolorization and subsequently the mineralization of Acid Blue 80 in model dyeworks wastewater, both in the homogeneous phase using the Fenton and photo-Fenton reactions, UV-C and UVC/H₂O₂ processes, and in the heterogeneous phase, where the proven commercial photocatalysts P25, P90, and AV01 based on TiO₂ were used. The influence of pH of the environment was studied and in the case of the Fenton reaction, the influence of the concentration of catalyzing Fe²⁺ ions on the rate of decolorization of the model wastewater was also studied. The optimal molar ratio of H₂O₂/Fe²⁺ was 10:1. For describing the reaction kinetics, first-order speed constants were best-suited. In all applied processes, the dye chromophore degraded, which was accompanied by a quantitative decolorization of the model wastewater. Subsequently, the mineralization of colorless intermediate products was studied through a decrease in COD or, more precisely, TOC. The mineralization efficiency in the homogeneous phase ranged between 18.6 and 97.1% after 24 h. In the case of heterogeneous photocatalysis, it ranged between 79.6 and 97.3% after 24 h, with efficiency declining in the order P90 > P25 > AV01.

Keywords: Acid Blue 80; Fenton oxidation; dye photolysis; photocatalytic oxidation



Citation: Palarčík, J.; Krupková, O.; Peroutková, P.; Malaťák, J.; Velebil, J.; Chýlková, J.; Dušek, L. Decolorization and Oxidation of Acid Blue 80 in Homogeneous and Heterogeneous Phases by Selected AOP Processes. *Catalysts* **2022**, *12*, 644. <https://doi.org/10.3390/catal12060644>

Academic Editor: Antonio Eduardo Palomares

Received: 29 April 2022

Accepted: 8 June 2022

Published: 12 June 2022

Publisher's Note: MDPI stays neutral with regard to jurisdictional claims in published maps and institutional affiliations.



Copyright: © 2022 by the authors. Licensee MDPI, Basel, Switzerland. This article is an open access article distributed under the terms and conditions of the Creative Commons Attribution (CC BY) license (<https://creativecommons.org/licenses/by/4.0/>).

1. Introduction

The textile and dye industry all over the world is mostly expanding in densely populated developing countries where it substantially contributes to the pollution of rivers and, by extension, oceans [1,2]. The wastewater from the industrial branches is typically contaminated with organic dyes, detergents, and auxiliary textile agents as well as a high concentration of sodium chloride, sulfate, or carbonates [3]. Such a combination usually makes degradation of the contaminants difficult, which results in the low self-cleaning abilities of the contaminated water and the insufficient efficiency of biological-mechanical wastewater treatment plants. In view of this, it is useful to study the sub-processes and develop commercially and environmentally friendly multi-stage wastewater treatment technologies. Advanced oxidation processes (AOP), using in situ production of highly reactive hydroxyl radicals ($\bullet\text{OH}$) [4–7], are usually applied for the oxidation of the organic matrix of pollutants. They are some of the strongest oxidizing agents and can be used in aquatic environments. They are characterized by a non-selective course of oxidation, where the reaction rate is usually controlled by diffusion. When compared with other conventional oxidants ($E^\circ(\text{O}_3) = 2.08\text{ V}$, $E^\circ(\text{H}_2\text{O}_2) = 1.78\text{ V}$, $E^\circ(\text{KMnO}_4) = 1.70\text{ V}$, $E^\circ(\text{Cl}_2) = 1.36\text{ V}$), hydroxyl radicals ($\bullet\text{OH}$) have a high standard reproduction potential ($E^\circ = 2.80\text{ V}$). Only fluor ($E^\circ = 3.06\text{ V}$) has a higher value of E° , see Refs. [8,9], and, depending on the conditions, also sulfate radical $\text{SO}_4^{\bullet-}$ ($E_0 = 2.5\text{--}3.1\text{ V}$), which is used in a lot of SR-AOPs [10]. When

compared with $\bullet\text{OH}$, its specific advantage is its longer half-life ($t_{1/2} = 30\text{--}40 \mu\text{s}$), which brings a particular advantage in environments with higher concentrations of carbonates or phosphates [11].

Our kinetic study builds on our previous paper [12] in which we compared the indirect electrochemical oxidation of Acid Blue 80 (AB 80) on active Pt and non-active BDD anodes and proposed a reaction mechanism for the degradation of this dye using $\bullet\text{OH}$ in the presence and absence of chloride ions. Again, we used AB80 and performed kinetic experiments monitoring the decolorization rate, i.e., the degradation of dye chromophore and the subsequent partial/total mineralization of intermediate products in homogeneous and heterogeneous phases [4,13] at comparable concentrations of AB80 and within the same range of pH 3–11. In general, it can be stated that hydroxyl radicals can be generated both by using a combination of more primary oxidants (e.g., ozone, hydrogen peroxide, oxygen), and also by using a DC power supply and passive electrodes, e.g., BDD electrodes and/or solar energy sources (e.g., ultraviolet light) and catalysts (e.g., titanium white). To decompose AB80 dye in the homogeneous phase, we used the Fenton and photo-Fenton oxidations, photolytic decomposition of AB80 using UV-C radiation, as well as the UVC/ H_2O_2 reaction system. At the same time, we subjected AB80 to photochemical oxidation in the heterogeneous phase. In this case, we chose the $\text{TiO}_2/\text{UVA}/\text{O}_2$ reaction system and selected the commercially available, non-toxic, cheap, and well-tried anatase TiO_2 photocatalysts P25, P90, and AV01 [14–17]. When selecting them, we were inspired by papers that prove that TiO_2 photo-catalysis may cause the decolorization of various dyes, such as Acid Blue 80 [18–20], Acid Orange 52 [21,22], Reactive Red 239 [23], and many others. Table 1 summarizes the reaction mechanisms of the creation of $\bullet\text{OH}$ in the applied processes used for the decolorization and oxidation of AB80.

Table 1. Overview of AOP processes and their mechanisms of generating hydroxyl radicals.

AOP Process Name	Reaction System	System Reaction Mechanism	Ref.
Fenton oxidation	$\text{H}_2\text{O}_2/\text{Fe}^{2+}$	$\text{Fe}^{2+} + \text{H}_2\text{O}_2 \rightarrow \text{Fe}^{3+} + \text{OH}^- + \text{OH}\bullet$ $\text{Fe}^{3+} + \text{H}_2\text{O}_2 \rightarrow \text{H}^+ + \text{Fe-OOH}^{2+}$ $\text{Fe-OOH}^{2+} \rightarrow \text{HO}_2\bullet + \text{Fe}^{2+}$	[9,24–27]
Photo-Fenton oxidation	$\text{H}_2\text{O}_2/\text{Fe}^{2+}/\text{UV}$ $\text{H}_2\text{O}_2/\text{Fe}^{3+}/\text{UV}$ $\text{H}_2\text{O}_2/[\text{Fe}^{\text{III}}(\text{C}_2\text{O}_4)_3]^{3-}/\text{UV}$	$\text{Fe}^{2+} + \text{H}_2\text{O}_2 \rightarrow \text{Fe}^{3+} + \text{OH}^- + \text{OH}\bullet$ $\text{Fe}(\text{OH})^{2+} + h\nu \rightarrow \text{Fe}^{2+} + \text{OH}\bullet$ $\text{Fe}^{3+} + \text{H}_2\text{O}_2 \rightarrow \text{Fe}^{2+} + \text{HO}_2\bullet + \text{H}^+$ $[\text{Fe}^{\text{III}}(\text{C}_2\text{O}_4)_3]^{3-} + h\nu \rightarrow [\text{Fe}^{\text{II}}(\text{C}_2\text{O}_4)_2]^{2-} + \text{C}_2\text{O}_4^{\bullet-}$ $\text{C}_2\text{O}_4^{\bullet-} + [\text{Fe}^{\text{III}}(\text{C}_2\text{O}_4)_3]^{3-} \rightarrow [\text{Fe}^{\text{II}}(\text{C}_2\text{O}_4)_2]^{2-} + \text{C}_2\text{O}_4^{2-} + 2\text{CO}_2$ $\text{C}_2\text{O}_4^{\bullet-} + \text{O}_2 \rightarrow \text{O}_2^{\bullet-} + 2\text{CO}_2$	[28–30]
Photolysis	AB80/UVC	$\text{AB80} + h\nu \rightarrow \text{AB80}^{\bullet+} + e^-_{\text{aq}}$ $e^-_{\text{aq}} + \text{O}_2 \rightarrow \text{O}_2^{\bullet-} \quad k = 2 \times 10^{10} \text{ dm}^3\text{mol}^{-1}\text{s}^{-1}$ $2\text{O}_2^{\bullet-} + 2\text{H}_2\text{O} \rightarrow 2\text{OH}\bullet + \text{OH}^- + \text{O}_2$	[31,32]
Photochemical oxidation	$\text{H}_2\text{O}_2/\text{UVC}$	$\text{H}_2\text{O}_2 + h\nu \rightarrow 2\text{OH}\bullet$ $2\text{H}_2\text{O}_2 + 2\text{OH}\bullet \rightarrow \text{H}_2\text{O} + \text{HO}_2\bullet$ $2\text{HO}_2\bullet \rightarrow \text{H}_2\text{O} + \text{O}_2$	[33,34]
Photocatalytic oxidation	$\text{TiO}_2/\text{UVA}/\text{O}_2$	$\text{TiO}_2 + h\nu \rightarrow e^- + \text{TiO}_2(h^+)$ $e^- + \text{O}_2 \rightarrow \text{O}_2^{\bullet-}$ $2\text{O}_2^{\bullet-} + 2\text{H}_2\text{O} \rightarrow 2\text{OH}\bullet + \text{OH}^- + \text{O}_2$ $\text{TiO}_2(h^+) + \text{OH}^- \rightarrow \text{TiO}_2 + \text{OH}\bullet$ $\text{TiO}_2(h^+) + \text{H}_2\text{O} \rightarrow \text{TiO}_2 + \text{OH}\bullet + \text{H}^+$	[34–39]

2. Results

From the kinetic experiments of the decolorization of AB80 dye solutions, we obtained time dependences of absorbance from which current concentrations of AB80 were calculated as a function of time using the calibration line equation $A_{627} = 0.148c_{\text{AB80}} + 0.091$, $r^2 = 0.998$,

see Ref. [12]. Even though we also tried to apply zero- and second-order kinetic equations, in line with a number of analogous studies [40–44] and our assumptions, the first-order speed constants proved best to describe the acquired dependences.

It can be stated that the decolorization of AB80 was performed quantitatively in the homogeneous phase regardless of the selected reaction system in the entire tested pH range. This is also apparent in Figure 1A–D, which describe the efficiency of AB80 decolorization for the reaction systems of Fenton oxidation, photo-Fenton oxidation, simple photolysis, as well as photochemical oxidation in the presence of hydrogen peroxide.

When decolorizing AB80 solutions using Fenton oxidation, the effect of the ratio of the catalytic Fe^{2+} ions to the amount of hydrogen peroxide was also studied. A series of kinetic experiments taking place at pH = 3 and molar ratios $\text{Fe}^{2+}/\text{H}_2\text{O}_2 = 0, 1/5, 1/10, 1/25, 1/50, 1/75, 1/100, 1/200, \text{ and } 1/300$ showed that the decolorization of AB80 also takes place without the presence of Fe^{2+} ion but the corresponding rate constant is $k = 5.65 \times 10^{-5} \pm 1.15 \times 10^{-6} \text{ s}^{-1}$. The maximum decolorization rate was reached at the ratio $\text{Fe}^{2+}/\text{H}_2\text{O}_2 = 1/10$ when the rate constant achieved the value $= 1.04 \times 10^{-2} \pm 2.05 \times 10^{-4} \text{ s}^{-1}$. The dependence of first-order rate constants on the molar ratio of $\text{Fe}^{2+}/\text{H}_2\text{O}_2$ is shown in Figure 2A. The following Figure 2B illustrates the influence of the pH environment in the range between 3 and 11 on the AB80 decolorization rate.

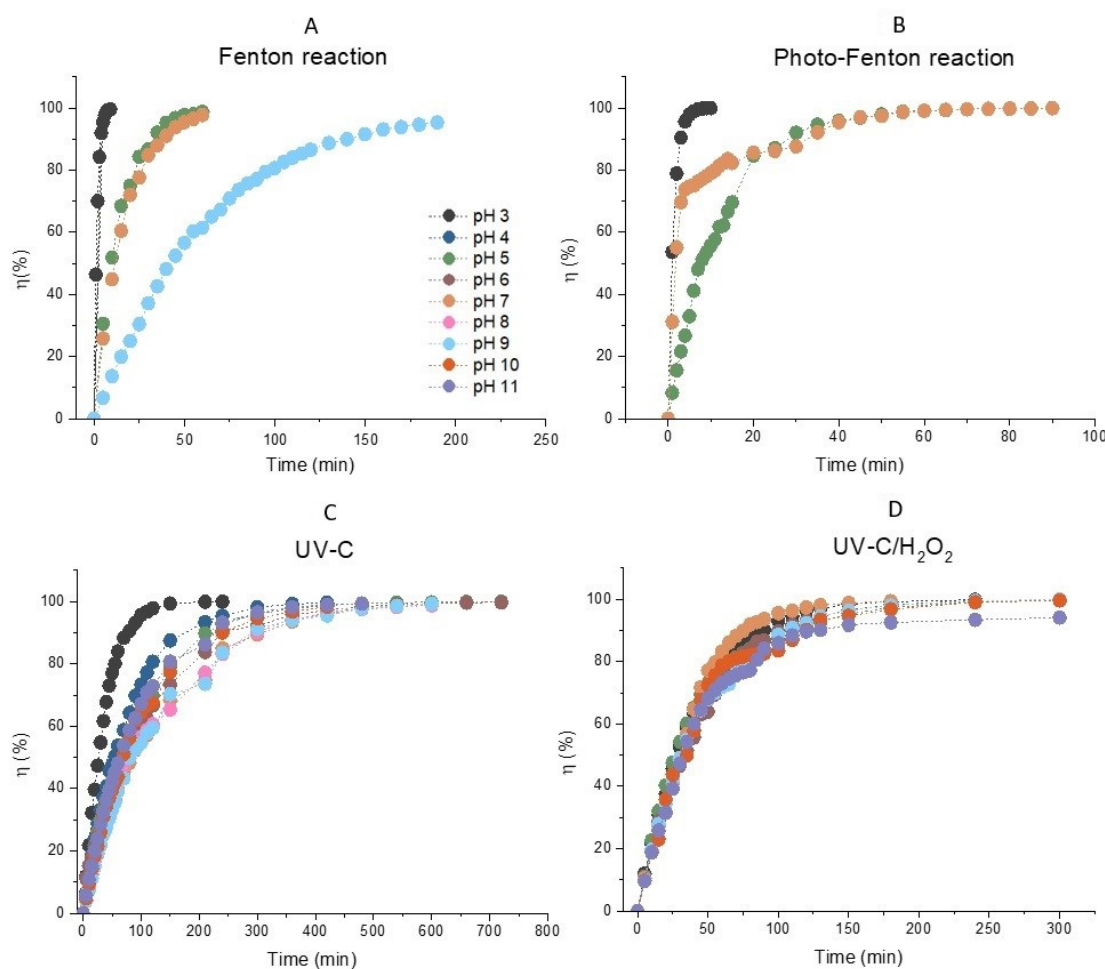


Figure 1. The dependences of efficiency of decolorization of model wastewater containing Acid Blue 80 over time in the homogeneous phase for the reaction systems. (A) Fenton oxidation ($\text{H}_2\text{O}_2/\text{Fe}^{2+}$), (B) photo-Fenton oxidation ($\text{H}_2\text{O}_2/\text{Fe}^{2+}/\text{UV}$), (C) simple photolysis AB80 UVC, (D) photochemical oxidation ($\text{UVC}/\text{H}_2\text{O}_2$). The initial concentration of AB80 was $1 \times 10^{-4} \text{ mol/L}$. The spectrophotometric kinetic measurements were done at $t = 25 \text{ }^\circ\text{C}$, $\lambda_{\text{anal}} = 627 \text{ nm}$ and in the pH range 3–11.

Apart from AB80 decolorization, we also studied the course of dye oxidation/mineralization in the homogeneous phase with pH = 3 using the time dependences of a change in COD and TOC. Based on the obtained data, we calculated the efficiency of AB80 chemical oxidation and mineralization according to relationship (2) depending on the time for the acidic environments, as seen in Figure 2C,D.

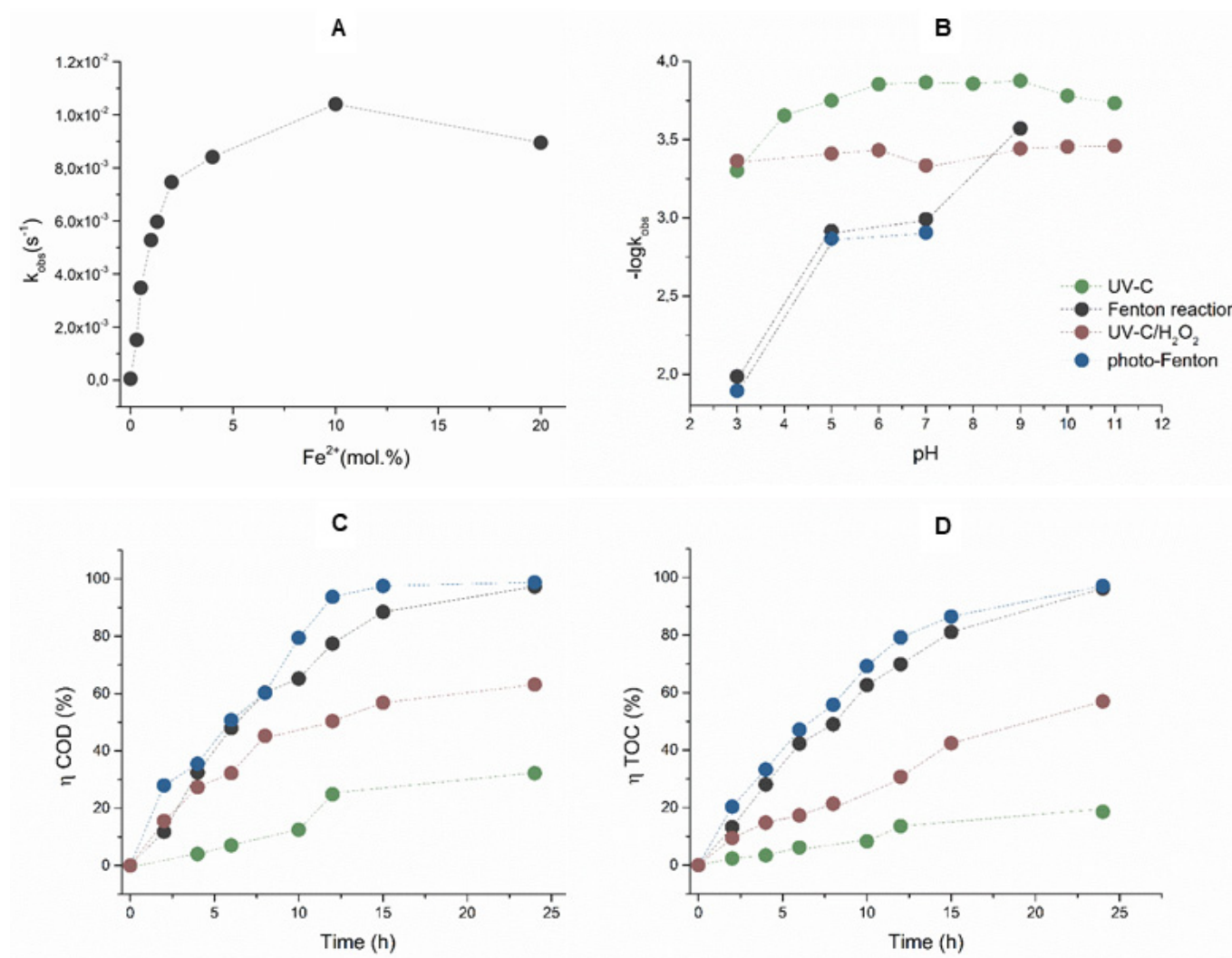


Figure 2. (A) Dependences of the observed first-order rate constant of the Fenton oxidation of AB80 on the molar ratio of Fe²⁺/H₂O₂ at pH = 3, $\lambda_{anal} = 627$ nm. (B) pH profiles of the H₂O₂/Fe²⁺, H₂O₂/Fe²⁺/UV, AB80/UVC, and UVC/H₂O₂ reaction systems describing the reaction rates of AB80 decolorization in the homogeneous phase, $\lambda_{anal} = 627$ nm. (C) The efficiency of AB80 oxidation at pH = 3 in the homogeneous phase for the applied reaction systems, is expressed by a relative reduction in COD. (D) The efficiency of AB80 mineralization at pH = 3 is expressed by a relative reduction in COD. The kinetic measurements were performed at t = 25 °C.

Also, during the photocatalytic oxidation of AB80 that occurred in the heterogeneous phase of the reaction system TiO₂/UVA/O₂ in the presence of the photocatalysts P25, P90, and AV01, a virtually quantitative decolorization was achieved regardless of pH of the environment. This is apparent in Figure 3A–C, which describe the efficiency of AB80 decolorization in the heterogeneous phase for individual photocatalysts depending on the reaction time. Figure 3 clearly shows the dependence of the observed rate constants of AB80 decolorization on the pH environment with regard to the selected photocatalyst.

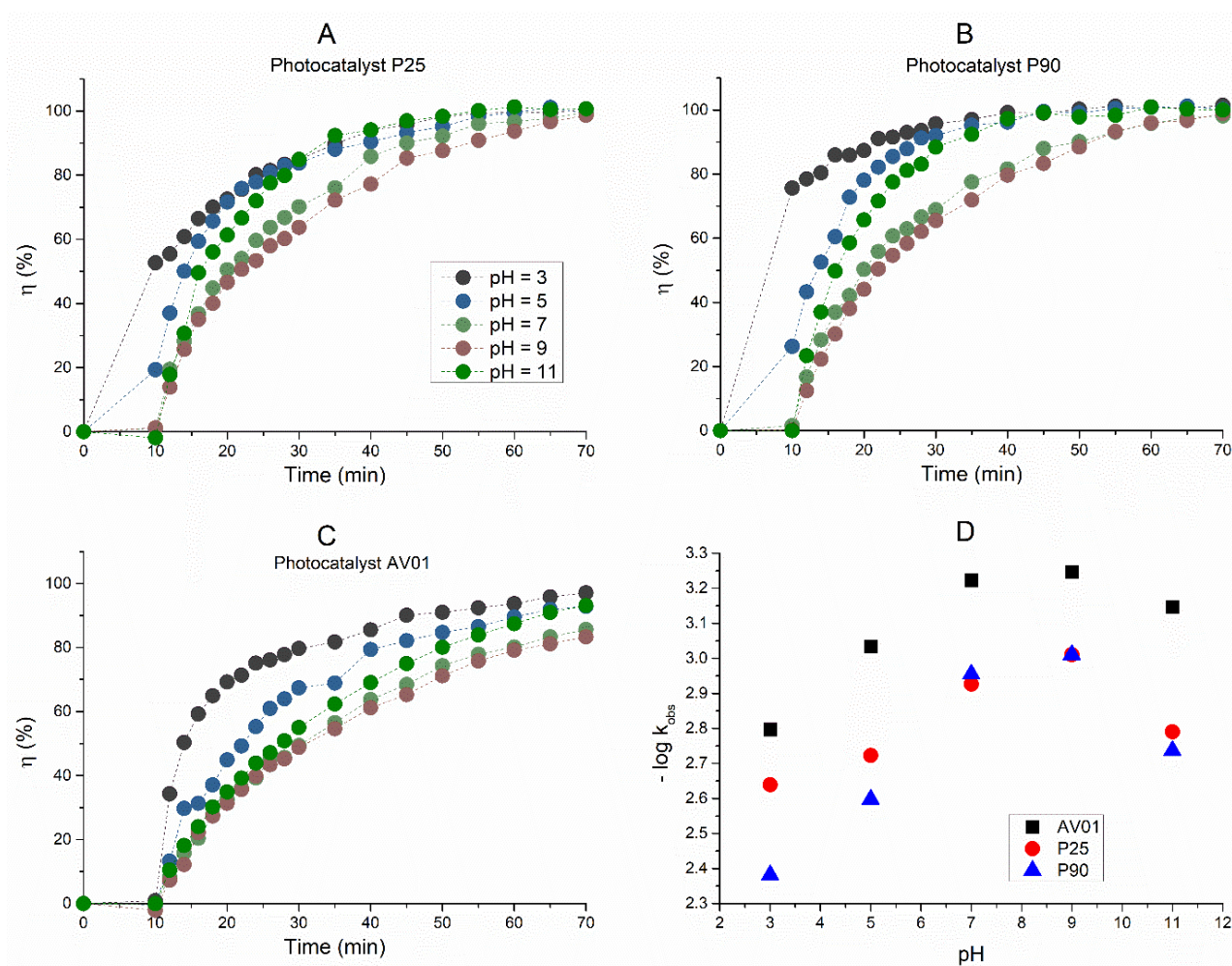


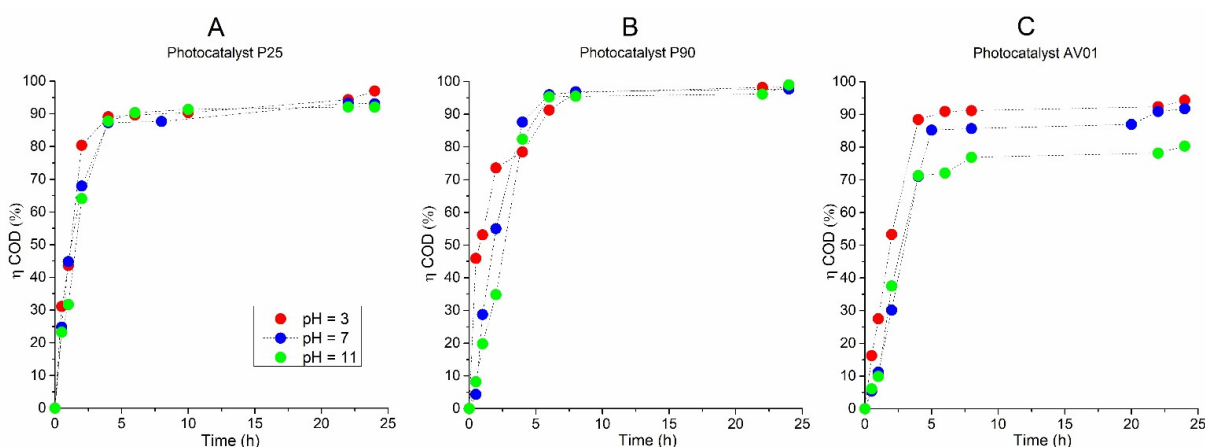
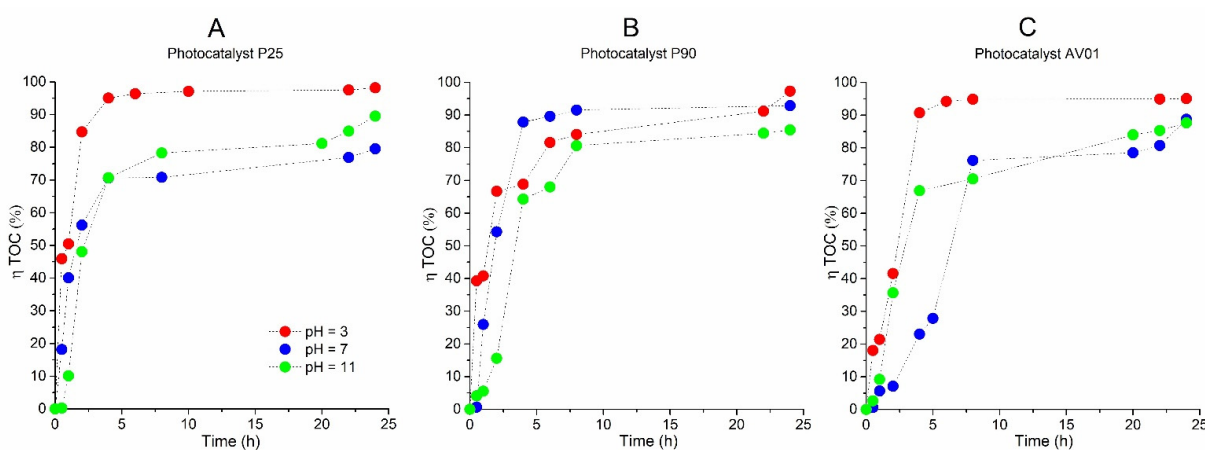
Figure 3. Dependence of the efficiency of decolorization of the model wastewater with Acid Blue 80 on the time of photocatalytic oxidation in the heterogeneous phase for photocatalysts (A) P25, (B) P90, and (C) AV01. (D) pH profiles of photocatalytic oxidation in the heterogeneous phase for photocatalysts P25, P90, and AV01. The initial concentration of AB80 was 1×10^{-4} mol/L. The spectrophotometric kinetic measurements were performed at $t = 25$ °C, $\lambda_{anal} = 627$ nm, and at a pH ranging from 3 to 11.

A comprehensive overview of the rates of the decolorization and mineralization of the model wastewater with AB80 for the reaction systems we selected in the homogeneous and the heterogeneous phases is shown in Table 2.

Simultaneously with the spectrophotometric measurement of the decrease in the AB80 absorbance/concentration in the model wastewater, the dependences of the COD and TOC decreases over time were obtained and the relative efficiency of AB80 oxidation and mineralization into carbon dioxide and water, respectively, were calculated. The dependences are described in Figures 4 and 5.

Table 2. Overview of the rate constants of the pseudo-first-order for AB80 decolorization and mineralization, depending on pH of the environment for various reaction systems at $t = 25\text{ }^{\circ}\text{C}$.

Process	Fenton	Foto-Fenton	UVC	UVC/H ₂ O ₂	Katalyst P25	UVA/TiO ₂ Katalyst P90	Katalyst AV01
pH	$k_1 \times 10^2$ (s ⁻¹)	$k_1 \times 10^2$ (s ⁻¹)	$k_1 \times 10^4$ (s ⁻¹)	$k_1 \times 10^4$ (s ⁻¹)	$k_1 \times 10^3$ (s ⁻¹)	$k_1 \times 10^3$ (s ⁻¹)	$k_1 \times 10^3$ (s ⁻¹)
Decolorization in a homogeneous phase				Decolorization in a heterogeneous phase			
3	1.04 ± 0.020	1.28 ± 0.029	4.99 ± 0.427	4.32 ± 0.196	2.29 ± 0.131	4.16 ± 0.292	1.60 ± 0.075
4	-	-	2.22 ± 0.599	-	-	-	-
5	0.12 ± 0.006	0.14 ± 0.008	1.78 ± 0.123	3.88 ± 0.200	1.89 ± 0.069	2.53 ± 0.072	0.93 ± 0.018
6	-	-	1.40 ± 0.033	3.70 ± 0.131	-	-	-
7	0.10 ± 0.002	0.12 ± 0.008	1.36 ± 0.061	4.63 ± 0.209	1.18 ± 0.021	1.11 ± 0.016	0.60 ± 0.006
8	-	-	1.39 ± 0.109	-	-	-	-
9	0.03 ± 0.001	-	1.33 ± 0.054	3.61 ± 0.141	0.98 ± 0.014	0.98 ± 0.010	0.57 ± 0.006
10	-	-	1.66 ± 0.061	3.51 ± 0.213	-	-	-
11	-	-	1.85 ± 0.038	3.47 ± 0.227	1.62 ± 0.011	1.84 ± 0.022	0.71 ± 0.007
Mineralization in a homogeneous phase				Mineralization in a heterogeneous phase			
3	0.16 ± 0.031	0.19 ± 0.033	1.67 ± 0.250	4.61 ± 0.635	0.21 ± 0.044	0.19 ± 0.074	0.13 ± 0.028
7	-	-	-	-	0.11 ± 0.023	0.11 ± 0.025	0.02 ± 0.003
11	-	-	-	-	0.08 ± 0.020	0.03 ± 0.004	0.03 ± 0.008

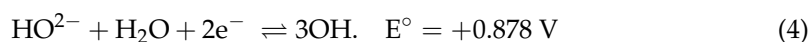
**Figure 4.** The efficiency of AB80 photocatalytic oxidation in the heterogeneous phase at $t = 25\text{ }^{\circ}\text{C}$, expressed by a relative decrease in COD: (A) P25, (B) P90, (C) AV01.**Figure 5.** The efficiency of AB80 photocatalytic mineralization in the heterogeneous phase at $t = 25\text{ }^{\circ}\text{C}$, expressed by a relative decrease in TOC: (A) P25, (B) P90, (C) AV01.

3. Discussion

As expected, the kinetic equations of the first or, more precisely, of the pseudo-first-order, are best suited to the measured kinetic data regardless of the reaction system. The pH profile for the Fenton oxidation of AB80 clearly shows that the reaction rate expressed by $k_{\text{obs}} = 1.04 \cdot 10^{-2} \text{ s}^{-1}$ ($t_{1/2} = 67 \text{ s}$) is the highest at pH = 3, whereas the reaction rate more or less stagnates with the pH ranging between 5 and 7 ($t_{1/2} = 9.5\text{--}11.3 \text{ min}$) and it further drops at pH = 9, $k_{\text{obs}} = 2.68 \cdot 10^{-4} \text{ s}^{-1}$ ($t_{1/2} = 43.3 \text{ min}$). The decolorization or degradation of chromophore AB80 in the model wastewater, did not take place in a more alkaline area with pH = 11 even after 24 h. In connection with the observed drop in the reaction rate of the decolorization with the growing pH, we must realize that the resulting decolorization rate, expressed with the rate constant k_{obs} , consists of the partial oxidation processes of AB80 by hydrogen peroxide itself and at the same time also by the oxidation of $\bullet\text{OH}$. The k_{obs} can, therefore, be expressed as the contribution of both processes in terms of Equation (1):

$$k_{\text{obs}} = k_{\text{H}_2\text{O}_2} + k_{\text{OH}} \quad (1)$$

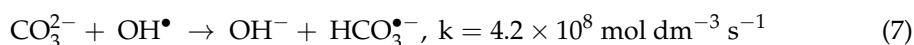
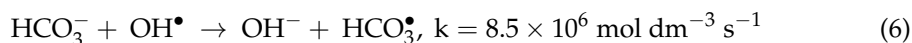
In the acidic pH range, where $E^\circ = 1.776 \text{ V}$, oxidation by using hydroxide peroxide within the meaning of Equation (2) is more effective. As the pH increases, the oxidation effect of peroxide decreases along with E° (see Equation (3)) and the deprotonated hydrogen peroxide acquires $E^\circ = +0.878 \text{ V}$ and -0.245 V , respectively, in an alkaline environment and finally becomes a reduction agent (see Equations (4) and (5); Ref. [45]).



During OH oxidation, its formation is conditioned by the simultaneous presence of H_2O_2 and the soluble form of the catalyzing Fe^{2+} ions. The concentration of dissolved and undissolved iron in water depends on the pH, the oxidation-reduction potential, and the presence of complex-forming substances. A part of the catalyzing Fe^{2+} ions are, however, oxidized to Fe^{3+} by dissolved oxygen. The concentration of the remaining Fe^{II} is limited by the solubility of $\text{Fe}(\text{OH})_2(\text{s})$ and $\text{FeCO}_3(\text{s})$. The solubility of $\text{Fe}(\text{OH})_2(\text{s})$ gradually decreases as the pH grows. The log is still $\text{cFe}(\text{OH})_2 = -1$ at $\text{pH} \approx 7$, the $\text{log cFe}(\text{OH})_2 = -5$ at $\text{pH} \approx 9$, and it reaches its minimum at $\text{pH} \approx 10.5\text{--}11.0$ when the $\text{log cFe}(\text{OH})_2 = -7$. As for the presence of carbon dioxide in water and the associated formation of $\text{FeCO}_3(\text{s})$, its effect both in the acidic and neutral range on the reaction rate of the Fenton reaction is negligible as its concentration is at least two orders lower. Moreover, it precipitates in the form of siderite from aqueous solutions very slowly and only after considerable supersaturation. In the alkaline range at $\text{pH} \geq 10.5$, $\text{FeCO}_3(\text{s})$ does not occur anymore and Fe^{II} is present in the form of $\text{Fe}(\text{OH})_2(\text{s})$. At the initial concentration of AB80 of circa $1 \times 10^{-4} \text{ mol/L}$ and the abundance of hydrogen peroxide, the decrease in the reaction rate of the Fenton reaction in the neutral and alkaline environments was caused by the low concentration of Fe^{2+} ions. This is compatible with the conclusions of a series of experiments studying the effects of the molar ratio of $\text{Fe}^{2+}/\text{H}_2\text{O}_2$ (0, 1/5, 1/10, 1/25, 1/50, 1/75, 1/100, 1/200, and 1/300). If no Fe^{2+} ions were added during oxidation, the AB80 decolorization rate only corresponded with the contribution of $k_{\text{H}_2\text{O}_2}$, when the equation is $k_{\text{obs}} = k_{\text{H}_2\text{O}_2} = 5.65 \cdot 10^{-5} \text{ s}^{-1}$ and $t_{1/2} \approx 3.4 \text{ h}$. The maximum decolorization rate is achieved at $\text{Fe}^{2+}/\text{H}_2\text{O}_2 = 1:10$, and then there is a drop, which is compatible with the conclusions made by Da Pozzo, Jiang, and Rosales [46–48]. The above conclusions also apply to the photo-Fenton oxidation and, due to the influence of an additional source of $\bullet\text{OH}$, the decrease in the reaction rate due to pH is somewhat reduced, as seen in Table 2.

When decolorizing AB80 using UV-C radiation, the highest rate was observed at pH 3 ($t_{1/2}$ was circa 23 min). Within the pH range between 6 and 9, the reaction rate decreased and the reaction half-time was around 83 min, whereas the corresponding reaction half-time was around 63 min in the alkaline range at pH = 11. In this case, the $\bullet\text{OH}$ precursor is the superoxide $\text{O}_2^{\bullet-}$ formed after the acceptance of an electron by singlet oxygen. Although a solution of AB80 is stable in daylight and the decolorization was not apparent even after 6 months, the quantitative degradation of the dye chromophore due to UVC photolysis was observed within the whole range of the pH profile.

The process can be sped up by the photochemical oxidation of AB80 with the UVC/ H_2O_2 system. The photoinduced decomposition of hydrogen peroxide generating hydroxyl radicals is independent, to a substantial degree, of the pH of the environment, and thus the AB80 decolorization rate is less dependent on the pH of the environment. This assumption was confirmed during the kinetic experiments, as the reaction half-time $t_{1/2}$ changed with the pH ranging between 3 and 11 from circa 27 min at pH = 3 to 33 min with pH \approx 10–11. In the case of model water with AB80 and the direct photolysis of AB80/UVC as well as the photochemical oxidation of UVC/ H_2O_2 , we explain the smaller slowdown of decolorization in the neutral and alkaline ranges by the presence of carbonates and bicarbonates catching the hydroxyl radical (Equations (6) and (7), Ref. [49]):



In the case of the heterogeneous photocatalytic oxidation of AB80 by the $\text{TiO}_2/\text{UVA}/\text{O}_2$ reaction system, the photocatalysis takes place in a series of partial steps, such as the transport of dissolved AB80 to the catalyst surface, its adsorption on the catalyst surface, the subsequent redox reaction, and the final desorption of the photocatalytic reaction products back to the liquid stage.

For this reason, it is also necessary to extend the simple kinetic model applied for the homogeneous oxidation of AB80. We chose a Langmuir–Hinshelwood model, which assumes the degradation of AB80 adsorbed on the catalyst surface [50,51]. The experimental data in all cases showed that the reaction rate was proportionate to c_{AB80} ($r \approx kKc_{\text{AB80}}$), and the reaction is regulated by first-order kinetics with a formal rate constant kK [52]. The observed rate constants shown in Table 2, therefore, include the adsorption coefficient for AB80. If we mutually compare the efficiency of the applied photocatalysts, the observed rate constants for the given pH environment correlate with their specific surface area in the order $\text{P90} > \text{P25} > \text{AV01}$. The corresponding half-times of decolorization at pH = 3 are 2.8 min (P90), 5 min (P25), and 7.2 min (AV01). In the neutral and alkaline ranges, there is a gradual slowdown in decolorization again with the trend culminating at pH \approx 9, as evidenced by the half-times 11.8 min (P90), 11.8 min (P25), and 20.3 min (AV01).

The AB80 oxidation and mineralization in the homogeneous phase were observed after the degradation of chromophore based on the decrease in COD and TOC only at pH \approx 3. Even though the AB80 decolorization in this environment is very fast, the oxidation of intermediary products is relatively slow, see Figure 2C,D. After circa 2 h of oxidation when the total decolorization of the model wastewater had already taken place, the level of TOC decreased depending on the reaction system by 5–8.9%, and it ranged between 32 and 43.6% after 12 h of AB80 mineralization. The situation in the heterogeneous phase for the individual catalysts is illustrated in Figures 4 and 5. The photocatalysts P90 showed the highest efficiency when the decrease in COD was achieved by 98.3% and the mineralization of AB80 dye took place from 97.3% at pH = 3 after 24 h of oxidation.

4. Materials and Methods

4.1. Chemicals and Materials

To prepare the model wastewater, textile aminoanthraquinone dye for wool and nylon, Acid Blue 80 (MW = 678.68 g/mol) with 90% purity (Synthesia a.s., Czech Republic) was

selected. Ferrous sulfate, used as a catalyst for the Fenton and photo-Fenton reactions, 30% hydrogen peroxide, sodium hydroxide, and 35% hydrochloric acid used in laboratory experiments as an oxidizing agent or for pH adjustment, were of analytical purity (Penta s.r.o., Czech Republic). Demineralized water with conductivity $\kappa \leq 4$ mS/cm was used to prepare the solutions.

TiO₂-based commercial photocatalysts, such as AEROXIDE[®] P 25 (specific surface (BET) 35–65 m²/g, produced by Evonik Industries AG, Hanau, Germany), AEROXIDE[®] P 90 (specific surface (BET) 70–110 m²/g, produced by Evonik Industries AG, Hanau, Germany), and AV-01 (specific surface (BET) 11–15 m²/g, produced by Precheza, a.s., Přerov, Czech Republic), were used for the photocatalytic degradation of AB80 in the heterogeneous phase.

4.2. Kinetic Measurements in a Homogeneous Phase

The apparatus for the kinetic experiments of AB80 decolorization and oxidation in the homogeneous phase consisted of an electromagnetic stirrer, a 5 L glass duplicator tempered at 25 °C with a Julabo EH-5 thermostat, and a source of UVC radiation, which was an EB-G45105 low-pressure mercury lamp (supplier: AQUA, Czech Republic) with a power input of 48 W (the total radiant power of the source was 13 W, the areal density of the radiant flux for 185 nm was 0.256 W/m², the areal density of the radiant flux for 254 nm was 1.20 W/m²). The UVC source was connected to the duplicator in a closed circulation circuit by a diaphragm pump with a bypass allowing it to regulate the flow in the range of 0–1.3 L/min. The kinetic experiments dependent on a UV source were carried out at a constant flow of $V = 0.33$ L/min. In the case of the Fenton oxidation, the UVC source was off, and the reaction took place directly on the stirred 5 L duplicator.

At the start of the kinetic experiment, the stirred duplicator was filled with 5 L of the model wastewater at an initial concentration $c = 1 \times 10^{-4}$ mol/L of AB80 dye, which was adjusted by adding 0.1 mol/L chlorine hydride or with 0.1 mol/L sodium hydroxide. The initial pH of the model wastewater for the kinetic experiments ranged between 3 and 11, and the pH was maintained during the experiments within ± 0.2 units using a two-channel automatic titrator TitraLab 856, programmed as a two-channel pH-stat. Subsequently, the solution was tempered at a temperature of 25 °C and 30% hydrogen peroxide, and a solution of ferrous sulfate was injected depending on the selected reaction system or, when necessary, when the source of the UVC radiation was switched on. At the same time, using a closed circuit created by the duplicator, a peristaltic pump, and a flow 10 mm quartz cuvette (flow $V = 5$ mL/min), the decrease in absorbance was monitored spectrophotometrically at $\lambda_{\text{anal.}} = 627$ nm depending on the time and until stabilization. Then, the dependence of the current concentration of AB80 on the time and the rate constant of the pseudo-first-order for the dye decolorization was calculated from the calibration curve. In the case of monitoring the AB80 oxidation and mineralization, the reaction time was extended to 24 h and samples were taken continuously from the reaction mixture to determine the current values of COD and TOC.

4.2.1. Fenton Oxidation

The initial AB80 concentration was 1×10^{-4} mol/L. A solution of 30% hydrogen peroxide was used in a 10% molar surplus over the necessary quantity for the overall mineralization of AB80 into carbon dioxide and water. The initial molar ratio of hydrogen peroxide and Fe²⁺ was 10:1. Under these conditions, the pH profile of AB80 oxidation was established within the range between 3 and 11. The influence of the molar ratio of Fe²⁺/H₂O₂ (1/0, 1/5, 1/10, 1/25, 1/50, 1/75, 1/100, 1/200, and 1/300) was further studied with a 10% molar surplus over AB80 at pH = 3.

4.2.2. Photo-Fenton Oxidation

The kinetic experiments were performed under identical conditions as in the Fenton oxidation, but before the hydrogen peroxide and ferrous sulfate mixture were added, the

UVC source was switched on during the tempering of the model wastewater. The pH profile of AB80 decolorization was established within the range of 3–7.

4.2.3. AB80 Photolysis Using UVC

The photolysis was performed only with a tempered sample of AB80 model wastewater. The pH profile of the dye decolorization was established in the range of 3–11.

4.2.4. Photochemical Oxidation of AB80 Using the UV-C/H₂O₂ Reaction System

The quantity of 30% hydrogen peroxide was in a 10% molar surplus over AB80, assuming total mineralization of the dye. The pH profile of the dye decolorization was developed within the range of 3–11. Subsequently, the AB80 oxidation–mineralization was studied only in an acidic environment with pH ≈ 3.

4.3. Kinetic Measurements in a Heterogeneous Phase

The apparatus for the kinetic experiments of AB80 decolorization and oxidation in the heterogeneous phase consisted of an electromagnetic stirrer, a 1 L reaction duplicator tempered at 25 °C with a Julabo EH-5 thermostat, and a UV radiation source, which was a UV-A LED lamp (supplier: Phoseon FireJet FJ100) with a radiation wavelength of 365 nm, providing a radiation flux of intensity 1.284 W/cm². The UVA source was placed over the duplicator and irradiated an area of 285.12 cm².

Before initiating the kinetic experiment, a model wastewater solution with an initial concentration of AB80 $c = 1 \times 10^{-4}$ mol/L was placed in the duplicator and its pH was adjusted within the range of 3–11 to the desired initial value, using 0.1 mol/L chlorine hydroxide (pH = 3 and 5) or 0.1 mol/L sodium hydroxide pH values 7, 9, and 11. Subsequently, the solution was tempered at a temperature of 25 °C. Then, a TiO₂-based selected photocatalyst was added so that its concentration was 1 g/L. The catalyst was dispersed with an electromagnetic stirrer (Heildolph MR Hei-tec) at 500 rpm for 10 min, then an initial model wastewater sample was taken and the UVA LED source was switched on. Subsequently, reaction samples were taken at defined intervals. They were then centrifuged (on an Eppendorf centrifuge 5804 R) at 11,000 rpm for 15 min, which separated them from the photocatalyst. Subsequently, the current concentration of AB80 was determined in the centrifuged samples using UV-VIS spectroscopy.

4.4. Calculations and Kinetic Models

For the reaction rate r of AB80 decolorization and oxidation in a homogeneous aqueous solution of the model wastewater, kinetic equations of the first- or, more precisely, of the pseudo-first-order, were best-suited, as seen in Equation (8) and Ref. [53]:

$$r = -\frac{dc_{AB80}}{dt} = k \times c_{AB80} \quad (8)$$

By solving it, we obtain Equations (9)–(11), which express the calculation of the observed rate constant k and the reaction half-time $t_{1/2}$:

$$\ln c_{AB80} - \ln c_{oAB80} = -k \times t \quad (9)$$

$$k = -\frac{\ln c_{AB80} - \ln c_{oAB80}}{t} \quad (10)$$

$$t_{1/2} = \frac{\ln 2}{k} \quad (11)$$

For the heterogeneous AB80 decolorization and oxidation taking place on the P25, P90, and AV01 photocatalyst surface after adsorption, we used the Langmuir–Hinshelwood kinetic model [49,50], as seen in Equation (12):

$$r = -\frac{dc_{AB80}}{dt} = \frac{k \times K \times c_{AB80}}{1 + K \times c_{AB80}} \quad (12)$$

where c_{AB80} is the molar concentration of degraded AB80, K is its adsorption coefficient on a TiO_2 surface, and k is the rate constant of dye degradation. The solution to Equation (12) can be written in the form of Equation (13):

$$\ln \frac{c_{tAB80}}{c_{oAB80}} + K \times (c_{tAB80} - c_{oAB80}) = -k \times K \times t = -k_{obs} \times t \quad (13)$$

In the case of a high concentration of AB80, $Kc_{AB80} \gg 1$ and the reaction rate are independent of the dye concentration. The decolorization rate is constant ($r \approx k$) and controlled by zero-order kinetics. On the contrary, if the initial AB80 concentration was $\leq 10^{-4}$ mol/L and $K \times c_{AB80} \ll 1$ during our kinetic measurements, the reaction rate r was proportional to c_{AB80} ($r \approx k \times K \times c_{AB80}$), and the reaction was controlled by first-order kinetics. Therefore, the observed rate constant given in Table 2 includes the relevant adsorption coefficient, $k_{obs} = k \times K$ [50].

We calculated the decolorization efficiency of the model wastewater containing AB80 according to Equation (14), also see Ref. [54]:

$$\eta(\%) = \left(1 - \left(\frac{c}{c_0}\right)\right) \times 100 \quad (14)$$

The COD and TOC removal efficiency, quantitatively describing the rate of AB80 oxidation and mineralization, respectively, was calculated analogously as a relative decrease in COD or TOC parameters compared to their initial values, as seen in Equations (15) and (16) and Ref. [54]:

$$\eta_{COD}(\%) = \left(1 - \left(\frac{COD_t}{COD_0}\right)\right) \times 100 \quad (15)$$

$$\eta_{TOC}(\%) = \left(1 - \left(\frac{TOC_t}{TOC_0}\right)\right) \times 100 \quad (16)$$

4.5. Analysis

The pH control and adjustment of model wastewater containing AB80 were performed using a pH meter (Accumet AB15 Basic, Fisher Scientific, Pensacola, FL, USA) or an automatic titrator TitraLab 856 (Radiometer analytical, Lyon, France). The electrolytic conductivity was controlled by conductometers (WTW Cond 3210 and WTW Cond 340i, Weilheim, Germany). UV-VIS spectra and dependences of absorbance versus time were measured on the UV-VIS spectrophotometers DR3900 and DR 6000 (Hach Lange GmbH, Düsseldorf, Germany). The initial and actual dye concentrations of AB80 were calculated from the absorbance values of the aqueous solutions at $\lambda_{anal} = 627$ nm and a temperature of 25 °C. The equation of the calibration line $A_{627} = 0.148c_{AB80} + 0.091$, $r^2 = 0.998$ was used for the calculation, as seen in Ref. [12].

The cuvette tests (HACH, Loveland, CO, USA) LCI 400 ISO 15705 (0–1000 mg/L), LCK514 (100–2000 mg/L), and LCK314 (15–150 mg/L) were used for the determination of chemical oxygen demand— COD_{Cr} —according to the methodology given in ISO 6060-1989, DIN 38409-H41-H44. The LT 200 thermoreactor (Hach Lange GmbH) was used to heat and temper (2 h at 148 ± 3 °C) the cuvette tests. Their evaluation was performed on a DR 2800 UV spectrophotometer (Hach Lange GmbH).

The determination of the total carbon content, TC, TIC, and TN was performed with the analyzer TOC/TN Formacs^{HT/TN} (Skalar Company, Breda, The Netherlands) using CSN EN 1484. The analyzer is equipped with two detectors: an NDIR detector for

the determination of carbon dioxide, and a chemiluminescence detector ND 25 for the determination of nitrogen. The standard solutions for calibration of the TOC/TN analyzer were prepared according to the rules in the EPA 415.2 and EPA 9060A methods.

5. Conclusions

The kinetic study builds on the previous paper [12] and compares the decolorization rate and the subsequent mineralization of Acid Blue 80 in model dyeworks wastewater. We applied the Fenton and photo-Fenton oxidations, simple UV-C photolysis, and photochemical UVC/H₂O₂ in a homogeneous solution of the dye and heterogeneous photocatalytic oxidation in the presence of TiO₂-based commercial photocatalysts P25, P90, and AV01. The Fenton and photo-Fenton oxidations were shown to be very sensitive to both the pH of the environment and the influence of the concentration of the catalyzing Fe²⁺ ions or, more precisely, the optimal molar ratio of H₂O₂/Fe²⁺, which was 10/1. The decolorization rate for these reaction systems ranged, depending on the conditions, between more than two orders, and the decolorization half-time was under 1 min below optimal conditions. The other reaction systems showed lower sensitivity to a change in reaction conditions, where the model wastewater decolorization rate slowed down circa 2–8 times compared to the ideal pH = 3. In the homogeneous phase, AB80 mineralization is relatively slow even under ideal conditions and 18.6–97.1% of AB80 was mineralized after 24 h. In the heterogeneous phase, the P90 photocatalyst proved to be the best allowing for mineralization of 97.3% at pH = 3 after 24 h, whereas the efficiency decreased in the order P90 > P25 > AV01. First-order rate constants were best-suited to describe the reaction kinetics of decolorization. During the experiments related to this publication, we did not discover any new intermediates or intermediates that would allow us to supplement or extend the AB80 degradation reaction mechanism proposed in the previous publication [12].

We are convinced that the mutual comparing of the kinetic data of AOP processes available in the industry for the selected problematic organic substrates allows a suitable choice of process and reaction conditions to be applied on an industrial scale. This enables the cheaper and more targeted local pre-treatment of problematic wastewater on a smaller scale using AOP processes and the subsequent final treatment in traditional mechanical–biological wastewater treatment plants. In this context, we are preparing a third follow-up publication dedicated to the issue of recycling AB80 from dyeing plants including dyeing tests. The intention is to compile an industrially usable technological sequence of recycling AB80 from dyeing baths and the subsequent final treatment of the generated wastewater by a selected AOP process in homogeneous or heterogeneous phases. We are convinced that the continuity of experimental conditions and the number of tested AOP processes will contribute to the higher modularity and usability of the obtained data in environmental protection on an industrial scale.

Author Contributions: Conceptualization, L.D. and J.P.; methodology, L.D. and J.P.; software, O.K. and J.M.; validation, O.K., P.P. and J.C.; formal analysis, J.C.; investigation, L.D.; resources, P.P. and O.K.; data curation, L.D. and J.P.; writing—original draft preparation, L.D.; writing—review and editing, L.D. and J.P.; visualization, P.P. and J.V.; supervision, L.D.; project administration, L.D.; funding acquisition, J.M. All authors have read and agreed to the published version of the manuscript.

Funding: This work was funded by the Ministry of Education, Youth and Sports of the Czech Republic, grant number SGS_2022_001.

Data Availability Statement: The data presented in this study are available on request from the corresponding author.

Conflicts of Interest: The authors declare no conflict of interest.

References

1. Chequer, F.M.D.; de Oliveira, G.A.R.; Ferraz, E.R.A.; Cardoso, J.C.; Zanoni, M.V.B.; de Oliveira, D.P. Textile Dyes: Dyeing Process and Environmental Impact. In *Eco-Friendly Textile Dyeing and Finishing*; Günay, M., Ed.; IntechOpen: London, UK, 2013. Available online: <https://www.intechopen.com/chapters/41411> (accessed on 7 April 2022). [CrossRef]
2. UNESCO World Water Assessment Programme. *Water for People, Water for Life: The United Nations World Water Development Report; A Joint Report by the Twenty-Three UN Agencies Concerned with Freshwater*, 1st ed.; UNESCO: Paris, France, 2003; pp. 85–87.
3. Yaseen, D.A.; Scholz, M. Textile dye wastewater characteristics and constituents of synthetic effluents: A critical review. *Int. J. Environ. Sci. Technol.* **2019**, *16*, 1193–1226. [CrossRef]
4. Uribe, I.O.; Mosquera-Corral, A.; Rodicio, J.L.; Esplugas, S. Advanced technologies for water treatment and reuse. *AIChE J.* **2015**, *61*, 3146–3158. [CrossRef]
5. Capodaglio, A.G. Critical Perspective on Advanced Treatment Processes for Water and Wastewater: AOPs, ARPs, and AORPs. *Appl. Sci.* **2020**, *10*, 4549. [CrossRef]
6. Cocha, M.; Farinelli, G.; Tiraferri, A.; Minella, M.; Vione, D. Advanced oxidation processes in the removal of organic substances from produced water: Potential, configurations, and research needs, *Chem. Eng. J.* **2021**, *414*, 128668. [CrossRef]
7. Cuerda-Correa, E.M.; Alexandre-Franco, M.F.; Fernández-González, C. Advanced Oxidation Processes for the Removal of Antibiotics from Water. An Overview. *Water* **2020**, *12*, 102. [CrossRef]
8. Pichat, P. *Photocatalysis and Water Purification: From Fundamentals to Recent Applications*, 1st ed.; Wiley-VCH: Weinheim, Germany, 2013; pp. 311–333.
9. Dušek, L. Treatment of wastewater using chemical oxidation with hydroxyl radicals. *Chem. List.* **2010**, *104*, 846–854.
10. Ren, W.; Zhou, Z.; Zhu, Y.; Jiang, L.; Wei, H.; Niu, T.; Fu, P.; Qiu, Z. Effect of sulfate radical oxidation on disintegration of waste activated sludge. *Int. Biodeter. Biodegrad.* **2015**, *104*, 384–390. [CrossRef]
11. Yang, Q.; Ma, Y.; Chen, F.; Yao, F.; Sun, J.; Wang, S.; Yi, K.; Hou, L.; Li, X.; Wang, D. Recent advances in photo-activated sulfate radical-advanced oxidation process (SR-AOP) for refractory organic pollutants removal in water. *Chem. Eng. J.* **2019**, *378*, 122149. [CrossRef]
12. Kuchtová, G.; Chýlková, J.; Váňa, J.; Vojs, M.; Dušek, L. Electro-oxidative decolorization and treatment of model wastewater containing Acid Blue 80 on boron doped diamond and platinum anodes. *J. Electroanal. Chem.* **2020**, *863*, 114036–114046. [CrossRef]
13. Lama, G.; Mejjide, J.; Sanromán, A.; Pazos, M. Heterogeneous Advanced Oxidation Processes: Current Approaches for Wastewater Treatment. *Catalysts* **2022**, *12*, 344. [CrossRef]
14. Schwarze, M.; Klingbeil, C.; Do, H.U.; Kutorglo, E.M.; Parapat, R.Y.; Tasbihi, M. Highly Active TiO₂ Photocatalysts for Hydrogen Production through a Combination of Commercial TiO₂ Material Selection and Platinum Co-Catalyst Deposition Using a Colloidal Approach with Green Reductants. *Catalysts* **2021**, *11*, 1027. [CrossRef]
15. Kete, M.; Pavlica, E.; Fresno, F.; Bratina, G.; Štangar, U.L. Highly active photocatalytic coatings prepared by a low-temperature method. *Environ. Sci. Pollut. Res.* **2014**, *21*, 11238–11249. [CrossRef] [PubMed]
16. Tolosana-Moranchel, A.; Casas, J.A.; Carbajo, J.; Faraldos, M.; Bahamonde, A. Influence of TiO₂ optical parameters in a slurry photocatalytic reactor: Kinetic modelling. *Appl. Catal. B Environ.* **2017**, *200*, 164–173. [CrossRef]
17. Keulemans, M.; Verbruggen, S.W.; Hauchecorne, B.; Martens, J.A.; Lenaerts, S. Activity versus selectivity in photocatalysis: Morphological or electronic properties tipping the scale. *J. Catal.* **2016**, *344*, 221–228. [CrossRef]
18. Espinola-Portilla, F.; Navarro-Mendoza, R.; Gutiérrez-Granados, S.; Morales-Muñoz, U.; Brillas-Coso, E.; Peralta-Hernández, J.M. A simple process for the deposition of TiO₂ onto BDD by electrophoresis and its application to the photoelectrocatalysis of Acid Blue 80 dye. *J. Electroanal. Chem.* **2017**, *802*, 57–63. [CrossRef]
19. Su, Y.; Deng, L.; Zhang, N.; Wang, X.; Zhu, X. Photocatalytic degradation of C.I. Acid Blue 80 in aqueous suspensions of titanium dioxide under sunlight. *React. Kinet. Catal. Lett.* **2009**, *98*, 227. [CrossRef]
20. Ao, C.H.; Leung, M.K.H.; Lam, R.C.W.; Leung, D.Y.C.; Vrijmoed, L.L.P.; Yam, W.C.; Ng, S.P. Photocatalytic decolorization of anthraquinonic dye by TiO₂ thin film under UVA and visible-light irradiation. *Chem. Eng. J.* **2007**, *129*, 153–159. [CrossRef]
21. Chen, C.; Wang, Z.; Ruan, S.; Zou, B.; Zhao, M.; Wu, F. Photocatalytic degradation of C.I. Acid Orange 52 in the presence of Zn-doped TiO₂ prepared by a stearic acid gel method. *Dye Pigment.* **2008**, *77*, 204–209. [CrossRef]
22. Galindo, C.; Jacques, P.; Kalt, A. Photodegradation of the aminoazobenzene acid orange 52 by three advanced oxidation processes: UV/H₂O₂, UV/TiO₂ and VIS/TiO₂: Comparative mechanistic and kinetic investigations. *J. Photochem. Photobiol. A Chem.* **2000**, *130*, 35–47. [CrossRef]
23. Saggiaro, E.M.; Oliveira, A.S.; Pavesi, T.; Maia, C.G.; Ferreira, L.F.V.; Moreira, J.C. Use of Titanium Dioxide Photocatalysis on the Remediation of Model Textile Wastewaters Containing Azo Dyes. *Molecules* **2011**, *16*, 10370–10386. [CrossRef]
24. Bello, M.M.; Aziz, A.; Raman, A.; Asghar, A. A review on approaches for addressing the limitations of Fenton oxidation for recalcitrant wastewater treatment. *Process Saf. Environ. Prot.* **2019**, *126*, 119–140. [CrossRef]
25. Brillas, E.; Garcia-Segura, S. Benchmarking recent advances and innovative technology approaches of Fenton, photo-Fenton, electro-Fenton, and related processes: A review on the relevance of phenol as model molecule. *Sep. Purif. Technol.* **2020**, *237*, 116337. [CrossRef]
26. Kočanová, V.; Dušek, L. Electrochemical dissolution of steel as a typical catalyst for electro-Fenton oxidation. *Mon. Chem.* **2016**, *147*, 935–941. [CrossRef] [PubMed]

27. Liu, Y.; Zhao, Y.; Wang, J. Fenton/Fenton-like processes with in-situ production of hydrogen peroxide/hydroxyl radical for degradation of emerging contaminants: Advances and prospects. *J. Hazard. Mater. Part B* **2021**, *404*, 124191. [CrossRef]
28. Kanafin, Y.N.; Makhatova, A.; Zariakas, V.; Arkhangelsky, E.; Pouloupoulos, S.G. Photo-Fenton-Like Treatment of Municipal Wastewater. *Catalysts* **2021**, *11*, 1206. [CrossRef]
29. Filice, S.; Bongiorno, C.; Libertino, S.; Gradon, L.; Iannazzo, D.; Scalese, S. Photo-Fenton Degradation of Methyl Orange with Dunino Halloysite as a Source of Iron. *Catalysts* **2022**, *12*, 257. [CrossRef]
30. Pouran, S.R.; Aziz, A.R.A.; Daud, W.M.A.W. Review on the main advances in photo-Fenton oxidation system for recalcitrant wastewaters. *J. Ind. Eng. Chem.* **2015**, *21*, 53–69. [CrossRef]
31. Buxton, G.V.; Greenstock, C.L.; Helman, W.P.; Ross, A.B. Critical-Review of Rate Constants for Reactions of Hydrated Electrons, Hydrogen-Atoms and Hydroxyl Radicals($\bullet\text{OH}/\bullet\text{O}^-$) in Aqueous-Solution. *J. Phys. Chem. Ref. Data* **1988**, *17*, 513–886. [CrossRef]
32. Wang, J.L.; Xu, J.L. Advanced Oxidation Processes for Wastewater Treatment: Formation of Hydroxyl Radical and Application. *Crit. Rev. Environ. Sci. Technol.* **2012**, *42*, 251–325. [CrossRef]
33. Krystynik, P.; Masin, P.; Kluson, P. Pilot scale application of UV-C/ H_2O_2 for removal of chlorinated ethenes from contaminated groundwater. *J. Water Supply Res. Technol. AQUA* **2018**, *67*, 414–422. [CrossRef]
34. Masin, P.; Krystynik, P.; Zebrak, R. Practical Application of Photochemical Oxidation H_2O_2 /UV-C Technique for Decontamination of Heavily Polluted Water. *Chem. Listy* **2015**, *11*, 885–891.
35. Tian, F.X.; Ye, W.K.; Xu, B.; Hu, X.J.; Ma, S.X.; Lai, F.; Gao, Q.Y.; Xing, H.B.; Xia, W.H.; Wang, B. Comparison of UV-induced AOPs (UV/ Cl_2 , UV/ NH_2Cl , UV/ ClO_2 and UV/ H_2O_2) in the degradation of iopamidol: Kinetics, energy requirements and DBPs-related toxicity in sequential disinfection processes. *Chem. Eng. J.* **2020**, *398*, 125570. [CrossRef] [PubMed]
36. Elmobarak, W.F.; Hameed, B.H.; Almomani, F.; Abdullah, A.Z. A Review on the Treatment of Petroleum Refinery Wastewater Using Advanced Oxidation Processes. *Catalysts* **2021**, *11*, 782. [CrossRef]
37. Sharma, K.; Vaya, D.; Prasad, G.; Surolia, P.K. Photocatalytic process for oily wastewater treatment: A review. *Int. J. Environ. Sci. Technol.* **2022**, *1*, 1–20. [CrossRef]
38. Zhang, Y.; Zhao, Y.G.; Maqbool, F.; Hu, Y. Removal of antibiotics pollutants in wastewater by UV-based advanced oxidation processes: Influence of water matrix components, processes optimization and application: A review. *J. Water Process Eng.* **2022**, *45*, 102496. [CrossRef]
39. Hama Aziz, K.H.; Omer, K.M.; Mahyar, A.; Miessner, H.; Mueller, S.; Moeller, D. Application of Photocatalytic Falling Film Reactor to Elucidate the Degradation Pathways of Pharmaceutical Diclofenac and Ibuprofen in Aqueous Solutions. *Coatings* **2019**, *9*, 465. [CrossRef]
40. Gupta, V.K.; Jain, R.; Mittal, A.; Saleh, T.A.; Nayak, A.; Agarwal, S.; Sikarwar, S. Photo-catalytic degradation of toxic dye amaranth on TiO_2 /UV in aqueous suspensions. *Mater. Sci. Eng. C* **2012**, *32*, 12–17. [CrossRef]
41. Gupta, V.K.; Jain, R.; Nayak, A.; Agarwal, S.; Shrivastava, M. Removal of the hazardous dye—Tartrazine by photodegradation on titanium dioxide surface. *Mater. Sci. Eng. C* **2011**, *31*, 1062–1067. [CrossRef]
42. Selvaraj, A.; Sivakumar, S.; Ramasamy, A.K.; Balasubramanian, V. Photocatalytic degradation of triazine dyes over N-doped TiO_2 in solar radiation. *Res. Chem. Intermed.* **2013**, *39*, 2287–2302. [CrossRef]
43. Behnajady, M.A.; Modirshahla, N. Nonlinear regression analysis of kinetics of the photocatalytic decolorization of an azodye in aqueous TiO_2 slurry. *Photochem. Photobiol. Sci.* **2006**, *5*, 1078–1081. [CrossRef]
44. Aleboyeh, A.; Aleboyeh, H.; Moussa, Y. Decolorisation of Acid Blue 74 by ultraviolet/ H_2O_2 . *Environ. Chem. Lett.* **2003**, *1*, 161–164. [CrossRef]
45. Lindsay, S. Effect of Electrolyte pH on the Electrosynthesis of Hydrogen Peroxide on Carbon Blackbased Gas Diffusion Electrodes. Master's Thesis, Clemson University, Clemson, SC, USA, 2020. Available online: https://tigerprints.clemson.edu/all_theses/3384 (accessed on 9 June 2022).
46. Da Pozzo, A.; Ferrantelli, P.; Merli, C.; Petrucci, E. Oxidation efficiency in the electro-Fenton process. *J. Appl. Electrochem.* **2005**, *35*, 391–398. [CrossRef]
47. Jiang, C.; Zhang, J. Progress and prospect in electro-Fenton process for wastewater treatment. *Zhejiang Univ. Sci.* **2007**, *8*, 1118–1125. [CrossRef]
48. Rosales, E.; Pazos, M.; Longo, M.A.; Sanromán, M.A. Electro-Fenton decoloration of dyes in a continuous reactor: A promising technology in colored wastewater treatment. *Chem. Eng. J.* **2009**, *155*, 62–67. [CrossRef]
49. Zuo, Z.; Cai, Z.; Katsumura, Y.; Chitose, N.; Muroya, Y. Reinvestigation of the acid-base equilibrium of the (bi)carbonate radical and pH dependence of its reactivity with inorganic reactants. *Radiat. Phys. Chem.* **1999**, *55*, 15–23. [CrossRef]
50. Bouchaaba, H.; Bellal, B.; Trari, M. Removal of a Commercial Dye, Alizarin Red, by Solar Photocatalysis Involving the Heterosystem ZnO-SnO_2 . *Theor. Exp. Chem.* **2018**, *53*, 417–422. [CrossRef]
51. Kumar, K.V.; Porkodi, K.; Selvaganapathi, A. Constrain in solving Langmuir–Hinshelwood kinetic expression for the photocatalytic degradation of Auramine O aqueous solutions by ZnO catalyst. *Dye Pigment.* **2007**, *75*, 246–249. [CrossRef]
52. Atkins, P.W.; De Paula, J. *Atkins' Physical Chemistry*, 8th ed.; Oxford University Press: Oxford, NY, USA, 2006; pp. 839–845.
53. Štěrba, V.; Panchartek, J. *Reaction Kinetics in Organic Chemistry*; Univerzita Pardubice: Pardubice, Czech Republic, 1995; ISBN 80-7194-018-6.
54. Nordin, N.; Riyanto, S.F.M.; Othman, M.R. Textile Industries Wastewater Treatment by Electrochemical Oxidation Technique Using Metal Plate. *Int. J. Electrochem. Sci.* **2013**, *8*, 11403–11415.